Tumor Biology and Immunology

Cancer Research

Reactivation of Mutant-EGFR Degradation through Clathrin Inhibition Overcomes Resistance to EGFR Tyrosine Kinase Inhibitors

Ludovic Ménard, Nicolas Floc'h, Matthew J. Martin, and Darren A.E. Cross

Abstract

Tyrosine kinase inhibitors (TKI) targeting mutant EGFR in non–small cell lung cancer (NSCLC) have been successful to control cancer growth, but acquired resistance inevitably occurs, including mutations directly on EGFR, for example, T790M and C797S. Strategies to prevent such acquired mutations by reducing mutant-EGFR expression have met limited success. Here, we propose a new model of mutant-EGFR trafficking and demonstrate that clathrin inhibition induces rapid degradation across a large panel of endogenous mutant-EGFR (Ex19del, L858R, and Ex20Ins). This panel included mutant-EGFR (T790M) resistant to the first- and second-generation EGFR inhibitors and to the third-generation TKI osimertinib and occurs through both mutational (C797S) and nonmutational EGFR mechanisms. Clathrin-mediated endocytosis inhibition of mutant EGFR induced a macropinocytosis-dependent lysosomal pathway associated with a loss of mutant-EGFR–dependent signaling (pAKT, pERK). Moreover, induction of this macropinocytic pathway led to robust apoptosis-dependent death across all mutant-EGFR cell lines tested, including those resistant to TKIs. We, therefore, propose a novel strategy to target mutant-EGFR refractory to approved existing TKI treatments in NSCLC and where new treatment strategies remain a key area of unmet need.

Significance: These findings extend our mechanistic understanding of NSCLC mutant EGFR trafficking biology, the role that trafficking may play in resistance of mutant EGFR to tyrosine kinase inhibitors, and provide new therapeutic and biological insights to tackle this fundamental issue and improve benefit to patients. *Cancer Res; 78(12); 3267–79. ©2018 AACR.*

Introduction

Tumors expressing activating mutations of EGFR have been reported in up to 15% and 40% of cases of non–small cell lung cancer (NSCLC) in Western and Asian populations, respectively (1). The canonical in-frame exon 19 deletion (Ex19Del) and L858R point mutation in exon 21 account for approximately 90% of all EGFR mutations while exon 20 insertions (Ex20Ins) account for 4% to 10% (2, 3).

In contrast to most Ex20Ins, the canonical EGFR mutations are highly responsive to approved first- and second-generation EGFR-TKIs, gefitinib, erlotinib, and afatinib. Although about 70% of patients respond initially to the treatment, acquired resistance to these EGFR-TKIs arises in all patients within 9 to 15 months of treatment (4–6). The gatekeeper EGFR T790M mutation is the most common mechanism of resistance, detected in approximately 60% of progressing tumors following TKI response (7). Osimertinib is an approved third-generation irreversible EGFR-TKI that was developed to overcome resistance from T790M mutation (8). As with early generation TKIs, despite high response rates and durable benefit achieved in activating mutant EGFR tumors harboring T790M (L858R/T790M and Ex19Del/T790M), most patients will ultimately experience progressive disease due to subsequent acquired resistance. Although the mechanisms of osimertinib resistance are still being characterized, it is clear that a subset of patients have tumors that acquire another tertiary EGFR mutation, C797S, which prevents covalent binding of the drug and, therefore, renders mutant-EGFR refractory to osimertinib (9). This highlights the need for novel therapeutic strategies to target oncogenic mutant EGFR that will prevent emergence of such resistance mutations or will be able to inhibit tumors that have acquired these resistance mutations upon TKIs treatment.

In the canonical model of RTK endocytosis and trafficking, activated receptors are recruited to clathrin through adaptors, such as AP2 or β-arrestin. The clathrin-coated pit is cleaved and released into the cytoplasm through the action of the GTPase dynamin. Receptors are then transported to early endosomes from where receptors can be sorted to recycling endosomes or further traffic to late endosomes before being eventually degraded into lysosomes. Endocytosis of RTKs is not a mechanism of desensitization only as several receptors remain competent to signal on endosomes before their degradation (10–13) and it has become increasingly recognized that endosomes can serve as platforms for amplification and compartmentalization of signals emitted by RTKs (13, 14) that determine response specificity such as cell migration (15, 16) and cell survival (17).

Importantly, endocytosis of oncogenic mutant-RTKs such as MET is believed to contribute to their tumorigenic activity (18). EGFR endocytosis and trafficking (19, 20) and also dysregulation of endocytosis machinery components [huntingtin interacting protein 1 (HIP1), clathrin light chain b (CLTB) and adaptor protein complex 2 (AP2A1, AP2A2, AP2B1; refs. 21–23) have been associated with drug resistance and/or cancer.

IMED Oncology, AstraZeneca, Cambridge, Cambridgeshire, United Kingdom.

Note: Supplementary data for this article are available at Cancer Research Online (http://cancerres.aacrjournals.org/).

Current address for L. Ménard: Luxembourg Institute of Health, Department of Oncology, Val Fleuri, Luxembourg, Luxembourg.

Corresponding Authors: Ludovic Ménard, Luxembourg Institute of Health, 84, Val Fleuri, Luxembourg L-1526, Luxembourg. Phone: 352-26970-252; Fax: 352-26970-719; E-mail: Ludovic.Menard@lih.lu; and Darren A.E. Cross, Darren.Cross@astrazeneca.com

doi: 10.1158/0008-5472.CAN-17-2195

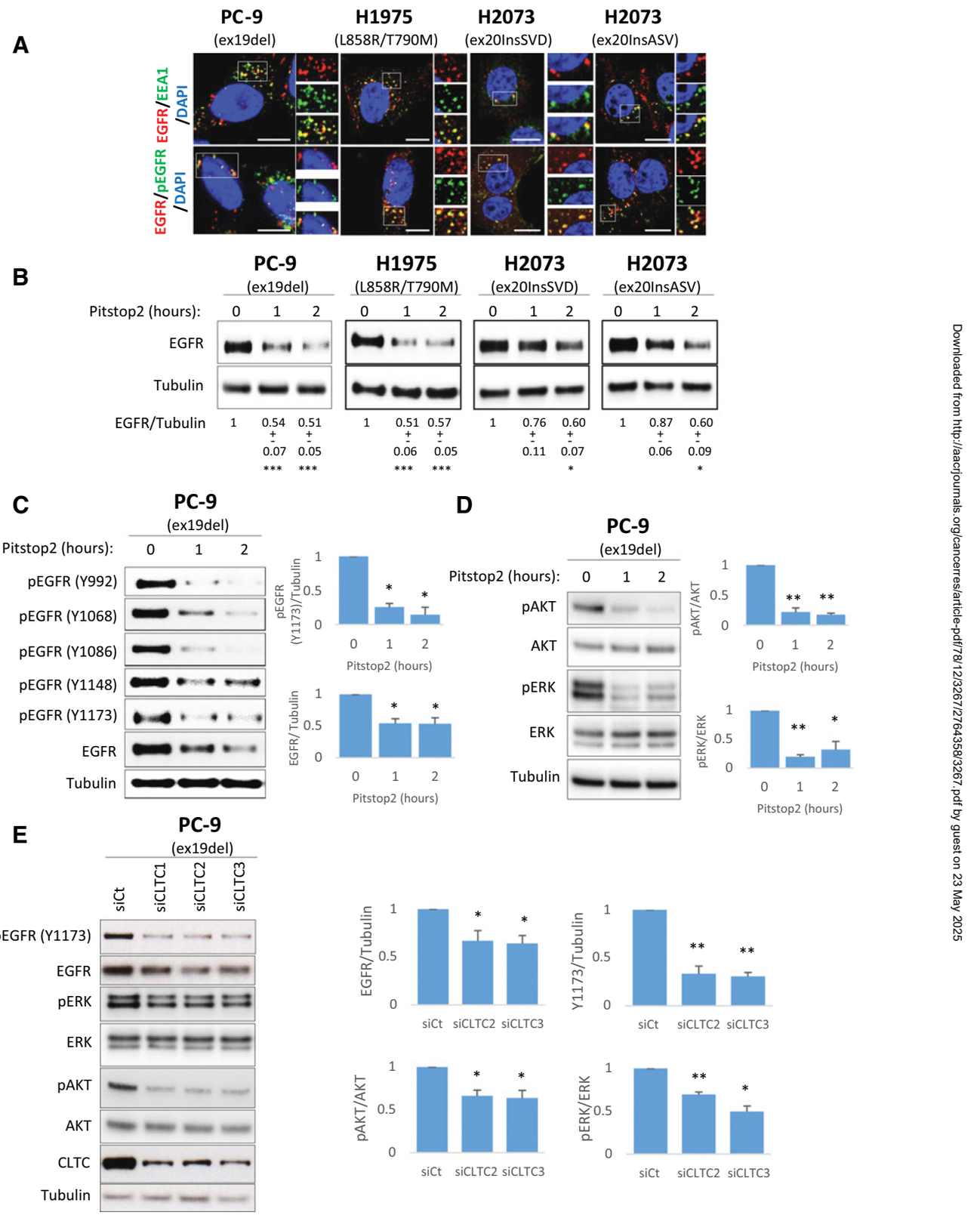

Although oncogenic-activating mutations of EGFR increase its internalization (24), they also prevent its degradation, which helps sustain its signaling (25). Despite mutant-EGFR endocytosis is believed to contribute to tumorigenesis, the molecular mechanisms of trafficking and endosomal signaling of mutant-EGFR in cancer remains poorly understood. Moreover, we hypothesized that more detailed understanding of mutant-EGFR endocytosis may reveal novel therapeutic strategies to tackle EGFR mutant-dependent TKI resistance mechanisms.

Here, using a cell line panel representative of different TKI-sensitive and resistance EGFR mutations, we show for the first time that clathrin inhibition diverts all mutant-EGFR to a macropinocytosis-dependent endocytosis pathway, which reroutes mutant-EGFR to lysosomal degradation. Inducing lysosomal mutant-EGFR degradation prevents receptor-dependent signaling and ultimately triggers apoptotic cell death. We thus report an alternative strategy to inhibit oncogenic activity of all types of TKI-sensitive and resistant mutant forms of EGFR.

Materials and Methods

Cell culture, transfection, RNA interference

PC-9 cells were obtained from European Collection of Authenticated Cell Cultures. NCI-H1975 and NCI-H2073 were obtained from ATCC. Cells were cultured in RPMI-1640 (Gibco) with 10% FCS (Gibco) and 2 mmol/L glutamine (Gibco) and maintained at 37°C in a humidified 5% CO_2 atmosphere. PC-9 and NCI-H1975 cell lines resistant to osimertinib were previously published (26). All cell lines were authenticated at AstraZeneca cell banking using DNA fingerprinting short-tandem repeat (STR) assays and confirmed to be free of *Mycoplasma*, bacterial and viral contaminations by IDEXX. All cell lines were used within 15 passages, and less than 2 months.

Transfections were carried out using Lipofectamine RNAi Max (Invitrogen) and ON-TARGETplus siRNAs (Dharmacon, Inc.) at a final concentration of 12.5 nmol/L for protein knock down. Clathrin heavy chain (CLTC) siRNAs: CLTC1 (J-004001-09), CLTC2 (J-004001-10), CLTC3 (J-004001-11). EGFR siRNAs: EGFR-1 (J-003114-12), siEGFR-2 (J-003114-13). Control siRNAs (D-001810-01-05).

Reagents

Osimertinib and gefitinib were synthesized according to published methods. Epidermal growth factor (EGF), tetramethylrhodamine conjugate (EGF-Tritc), Alexa Fluor 488 conjugate transferrin, alexa fluor 647 conjugate transferrin and Trypan blue solution (0.4%) were obtained from Thermo Fisher Scientific. Pitstop2, chloroquine diphospshate, Dyngo4a were obtained from Abcam. EIPA (5-(N-Ethyl-N-isopropyl)amiloride) was obtained from Sigma-Aldrich.

Primary antibodies used: rabbit polyclonals anti-EEA1 (Santa Cruz Biotechnology), -pEGFR(Y1086), -pEGFR(Y992), -pAKT, -AKT(S473), -pERK(T202/Y204), -MAPK1 (ERK), -pEGFR (Y1148), -pEGFR(Y1068), -CLTC, -MAP1LC3B (LC3b), -cleaved PARP1; rabbit monoclonal anti-EGFR, -p-EGFR(Y1173), -GAPDH, -cleaved caspase-3, -Lamp1 (all obtained from CST); mouse monoclonal anti-EGFR (Millipore), -TUBA4A (tubulin; Sigma-Aldrich); goat polyclonal anti-EEA1 (Santa Cruz Biotechnology). Secondary antibodies used for immunofluorescence: Alexa-488 labelled anti-rabbit, Alexa-555 labelled anti-mouse, and Alexa-647 anti-goat IgG (1/500, Molecular Probes); for Western blot: both anti-mouse and anti-rabbit IgG secondary antibodies were coupled to horseradish peroxidase (1/2,000, CST).

CRISPR cell line generation

CRISPR cell line generation was performed by transfecting cells using FuGENE HD (Promega; PC9 T790M/C797S) or electroporation following a standard Neon protocol (H2073 Ex20Ins) with a plasmid encoding Cas9-T2A-GFP and a guide specific to the site of insertion (PC9 T790M/C797S: ATGCCCTTCGGCTGCCTCC; H2073 Ex20Ins: CACGTGGGGGTTGTCCACGC). A synthetic PAGE ultramer ssDNA oligo with homology arms to EGFR Exon20 was cotransfected with the Cas9 plasmid at an equal ratio for PC9 T790M/C797S (donor sequence: GTGTGCCGCCTGCTGGGCA-TCTGCCTCACCTCCACCGTGCAGCTCATCATGCAGCTCATGCCC-TTCGGATCCCTCCTCGACTATGTCCGGGAACACAAAGACAATAT-TGGCTCCCAGTAC) or at ratio of 100:1 for H2073 Ex20Ins (donor sequence ASV: GAAGCCTACGTGATGGCCAGCGTGGCCAGCGT-GGAC AACCCCCACGTGTGCCGCCTGCTGGGCATCT; SVD: GAA-GCCTACGTGATGGCCAGC GTGGACAGCGTGGACAACCCCC-ACGTGTGCCGCCTGCTGGGCATCT) to the plasmid molarity. The donor oligo was designed to harbor (i) the relevant on-target point mutations (T790M/C797S) or exon 20 insertions (ASV and SVD), (ii) a silent mutation to increase both PCR assay detection efficiency and the generation of a restriction site for screening, and (iii) a silent mutation in the PAM site to prevent Cas9 recutting edited sequences. Cells were FACS sorted 48 hours after transfection and grown in media containing osimertinib (for PC9 T790M/C797S) or 10 nmol/L afatinib for 2 to 3 weeks before single-cell cloning. Single-cell clones were grown in 96 wells, DNA extracted by alkaline lysis and analyzed by ddPCR with specific probes. Clones positive for the specific mutation/insertion and negative for wild-type (WT) alleles were then sequenced to confirm the correct genome edit by Sanger sequencing.

Western blots and densitometry analysis

Cells were harvested in RIPA buffer containing a cocktail of protease and phosphatase inhibitors (Calbiochem). After protein quantification with the DC protein assay (Bio-Rad), 5 to 15 μg of

Figure 1.

Clathrin inhibition induces mutant-EGFR degradation and impairs its signaling. **A,** Confocal sections of indicated cells stained for EGFR (red), EEA1 (green), and DAPI (blue; top) or stained for EGFR (red), pEGFR (green), and DAPI (blue; bottom). pEGFR (Y1086) antibody was used for PC-9, NCI-H2073 Ex20InsSVD, NCI-H2073 Ex20InsASV cells, and pEGFR (Y1068) antibody was used for NCI-H1975 cells. Scale bar, 10 μm. **B,** Indicated cells were starved during 24 hours and treated or not with pitstop2 for 1 and 2 hours. Western blots for EGFR and tubulin were performed. Numbers represent mean EGFR/tubulin ratios ± SEM (PC9, $n = 6$; H1975, $n = 6$; H2073 ASV, $n = 3$; H2073 SVD, $n = 3$; *, $P < 0.05$; ***, $P < 0.001$, Student t test). **C,** PC-9 cells were starved during 24 hours and treated or not with pitstop2 for 1 and 2 hours. Western blots for pEGFR (Y992, Y1068, Y1086, Y1148, Y1173), EGFR, and tubulin were performed. Fold decreases over untreated are shown. Data, means ± SEM ($n = 3$; *, $P < 0.05$, Student t test). Quantification of pEGFR (Y1068, Y1086, Y1148) is shown in Supplementary Fig. S1l. **D,** PC-9 cells were starved during 24 hours and treated or not with Pitstop2 for 1 and 2 hours. Western blots for pAKT (S473), AKT, pERK (T202/Y204), ERK, and tubulin were performed. Fold decreases over untreated are shown. Data, means ± SEM ($n = 3$; *, $P < 0.05$; **, $P < 0.01$, Student t test). **E,** Cells were transfected with control or CLTC siRNAs. Western blots for pEGFR (Y1173), EGFR, pAKT, AKT, pERK, ERK, CLTC, and tubulin were performed. Fold decreases over siCt cells are shown for the two most efficient CLTC siRNAs. Quantification of CLTC knockdown is shown in Supplementary Fig. S1o. Data, means ± SEM [$n = 3$ for pERK, EGFR, pEGFR (Y1173); $n = 4$ for pAKT; *, $P < 0.05$; **, $P < 0.01$, Student t test].

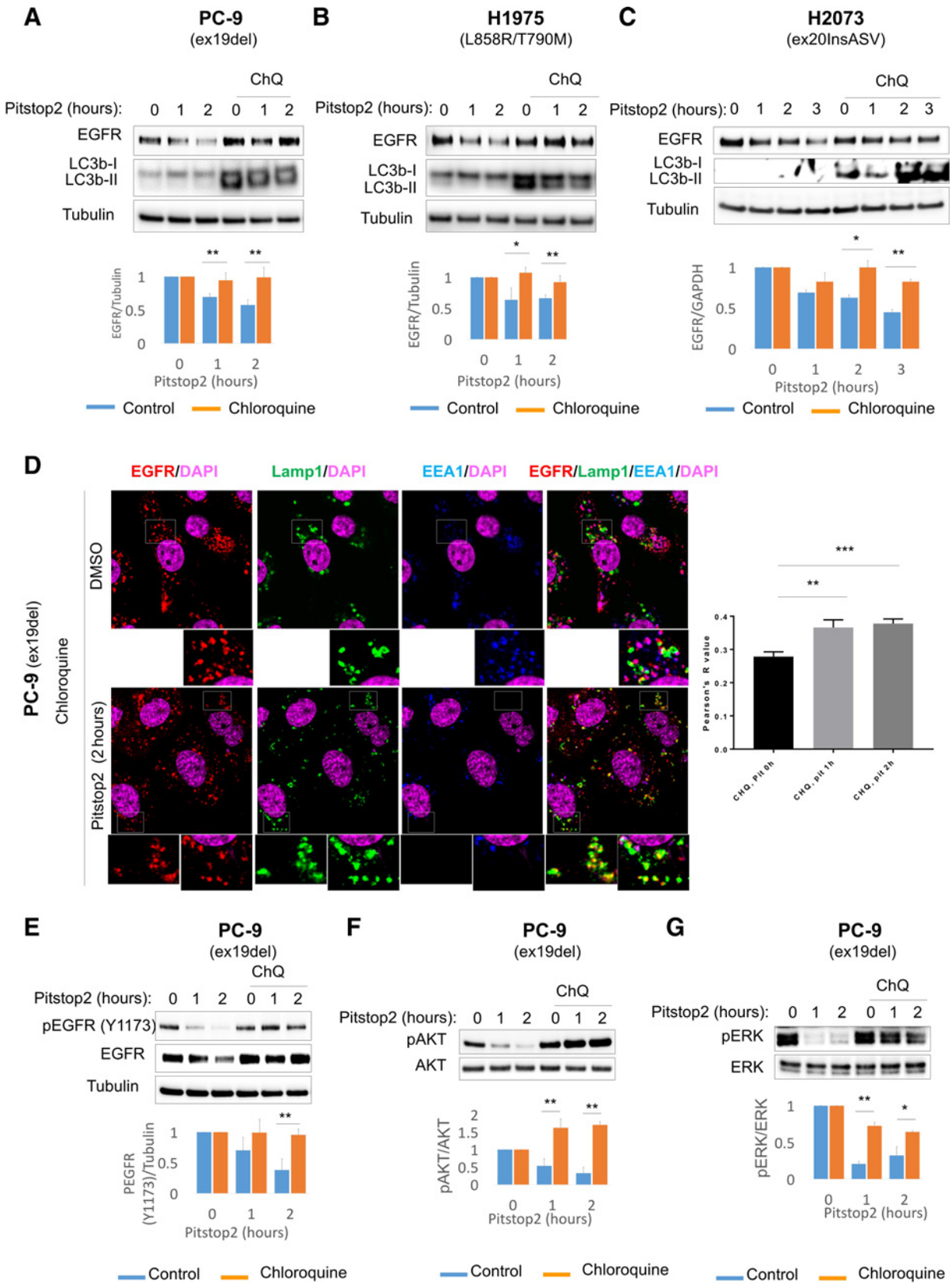

protein were resuspended in Laemmli sample buffer (CST) and boiled for 2 minutes. Samples were loaded on 4% to 12% gradient polyacrylamide gels (Invitrogen). Separated proteins were transferred to a 0.45-μm nitrocellulose transfer membrane (Whatman). Protein loading was checked by staining with Ponceau solution. Membranes were blotted with primary antibodies (1/1,000). Specific binding of antibodies was detected with peroxidase-conjugated secondary antibodies and visualized by enhanced chemiluminescence detection (Thermo Fisher Scientific). Densitometric analyses of immunoblots were performed using ImageJ 1.49 (National Institutes of Health).

Immunofluorescence and confocal microscopy analyses

Cells were plated in 24-well plates (3.5×10^4 per well) onto glass coverslips and 48 hours later, cells were starved 24 hours prior to pitstop2 incubation.

Immunofluorescence was performed as described previously (16). Briefly, cells were fixed with 4% PFA during 5 minutes, followed with NH_4Cl (50 mmol/L) incubation during 5 minutes. Cells were then permeabilized and blocked in phosphate buffer saline (PBS) containing 0.1% Triton-X100 and 2% BSA for 15 minutes. Primary and secondary antibodies were then incubated in PBS containing 2% BSA. ProLong Gold Antifade Mountant with DAPI was used (Thermo Fisher Scientific).

For EGF-Tritc uptake experiment, cells were pretreated with chloroquine (100 μmol/L) or EIPA (25 μmol/L) during 45 minutes, then treated with pitstop2 (30 μmol/L) during 15 minutes (37°C). Cells were then washed and incubated with cold PBS containing chloroquine or EIPA and pitstop2 in presence of EGF-TRITC during 40 minutes at 4°C in order to stain EGFR at the plasma membrane only. Cells were then washed to remove the nonbound EGF-Tritc and mutant-EGFR internalization was allowed by reincubating cells at 37°C during 5 and 10 minutes. Finally, cells were fixed with 4% PFA and analyzed by confocal microscopy.

Images were acquired using a Leica TCS SP5 inverted confocal microscope with x63 oil objective lenses. Laser power and gain were adjusted manually to give optimal fluorescence intensity for each fluorophore with minimal photobleaching. Each image corresponds to a single section of 0.8 μm thickness.

Pearson correlation coefficient was obtained with a colocalization analysis using Coloc 2 from ImageJ. Briefly, images to quantify were acquired randomly and for each ROI corresponding to every single cell, Pearson correlation coefficient between EGFR and Lamp1 was determined.

Cell viability

For trypan blue exclusion experiments, cells (1×10^5) were plated into 6-well plate during 72 hours. Cells were then starved during 24 hours and pretreated with chloroquine diphosphate (100 μmol/L) during 1 hour followed with pitstop2 (30 μmol/L) treatment during 3 hours. Cells were trypsinized and analyzed for viability by trypan blue exclusion.

For EGFR knockdown experiments, cells were transfected with siRNA as described above and 48 hours after transfection cells were plated at 2,000 cells/well in 96-well, white sides dishes. Cells were analyzed for viability 96 hours later using Cell Titer-Glo reagent (Promega) as per the manufacturer's instructions.

Cell confluency

Cells were plated into 48-well plate (7×10^3 per well for all isogenic cell lines except for PC9 $EGFR^{Ex19del/C797S}$ cells seeded at 14×10^3) in full media and maintained at 37°C in a humidified 5% CO_2 atmosphere. Forty-eight hours later, media were replaced with fresh media with 10% FCS containing or not DMSO, osimertinib (160 nmol/L) or gefitinib (160 nmol/L). The plates were placed in the Incucyte FLR (Essen Bioscience) at 37°C and imaged over 7 days at 4-hour time points incubated at 37°C, 5% $C0_2$ in the incucyte. The media with drug were replaced every 3 days.

Statistical analyses

Two-tailed Student *t* test was performed and paired between different conditions. Quantitative data are expressed as means ± SEM. Numbers are the results of at least three independent experiments. For EGF-Tritc uptake quantification, about 100 cells were counted in each condition. Cells were randomly chosen through the field by DAPI detection.

Results

Clathrin inhibition induces mutant-EGFR degradation and impairs its signaling

In order to investigate the localization and trafficking of the most common mutant-EGFR forms, we used a panel of NSCLC cell lines expressing different EGFR mutations: PC-9 (Ex19Del), NCI-H1975 (L858R/T790M), and the CRISPR-engineered NCI-H2073 (Ex20Ins) described previously (27). Consistent with previous reports, confocal microscopy immunofluorescence studies show that both $EGFR^{Ex19Del}$ and $EGFR^{L858R/T790M}$ are detected in intracellular vesicles and colocalize with the marker of early

Figure 2.

Clathrin inhibition induces mutant-EGFR degradation through lysosomal pathway. **A,** PC-9 cells were starved during 24 hours, pretreated or not with chloroquine (100 μmol/L) during 1 hour, and treated with pitstop2 (30 μmol/L) for 1 and 2 hours. Western blots for EGFR, LC3b, and tubulin were performed. Fold decreases over DMSO-treated cells are shown. Data, means ± SEM ($n = 5$; **, $P < 0.01$, Student *t* test). **B,** H1975 cells were starved during 24 hours, pretreated or not with chloroquine (100 μmol/L) during 1 hour and treated with pitstop2 (30 μmol/L) for 1 h and 2 hours. Western blots for EGFR, LC3b, and tubulin were performed. Fold decreases over DMSO-treated cells are shown. Data, means ± SEM ($n = 4$; *, $P < 0.05$; **, $P < 0.01$, Student *t* test). **C,** H2073 (Ex20InsASV) cells were starved during 24 hours, pretreated or not with chloroquine (100 μmol/L) during 1 hour, and treated with pitstop2 (30 μmol/L) for 1, 2, and 3 hours. Western blots for EGFR, LC3b, and tubulin were performed. Fold decreases over DMSO-treated cells are shown. Data, means ± SEM ($n = 3$ for 1 and 2 hours; $n = 4$ for 3 hours; *, $P < 0.05$; **, $P < 0.01$, Student *t* test). **D,** Confocal sections of PC-9 cells stained for EGFR (red), Lamp1 (green), EEA1 (blue), and DAPI (magenta). Cells were starved for 24 hours, pretreated with chloroquine (100 μmol/L) during 1 hour, and treated with pitstop2 (30 μmol/L) or DMSO during 2 hours. Scale bar, 10 μm. Quantification of EGFR and LAMP1 colocalisation is shown as Pearson coefficient. Data are mean ± SEM ($n = 28$ cells; **, $P < 0.005$; ***, $P < 0.001$; one-way ANOVA (Tukey test). **E,** PC-9 cells were starved during 24 hours and pretreated or not with chloroquine (100 μmol/L) during 1 hour and treated with pitstop2 (30 μmol/L) for 1 and 2 hours. Western blots for EGFR, pEGFR (Y1173), and tubulin were performed. Fold decreases over DMSO-treated cells are shown. Data, means ± SEM ($n = 5$; **, $P < 0.01$, Student *t* test). **F,** PC-9 cells were starved during 24 hours and pretreated or not with chloroquine (100 μmol/L) during 1 hour and treated with pitstop2 (30 μmol/L) for 1 and 2 hours. Western blots for pAKT and AKT were performed. Fold decreases over DMSO-treated cells are shown. Data, means ± SEM ($n = 4$; **, $P < 0.01$, Student *t* test). **G,** PC-9 cells were starved during 24 hours and pretreated or not with chloroquine (100 μmol/L) during 1 hour and treated with pitstop2 (30 μmol/L) for 1 and 2 hours. Western blots for pERK and ERK were performed. Fold decreases over DMSO-treated cells are shown. Data, means ± SEM ($n = 4$; *, $P < 0.05$; **, $P < 0.01$, Student *t* test).

endosomes EEA1 (Fig. 1A, top) whereas $EGFR^{WT}$ is mostly localized at the plasma membrane in H460 and A549 cell lines (Supplementary Fig. S1A). Similarly, the less characterized Ex20Ins SVD and ASV EGFR are localized in early endosomes. In all the cell lines tested, osimertinib-induced inhibition of pEGFR sites of the kinase domain suggest that mutant-EGFR are constitutively activated (Supplementary Fig. S1B–S1E). Potential ligand-dependent internalization was excluded as cells were starved during 24 hours before analysis. Moreover, internalized mutant EGFR are also activated as shown by confocal microscopy analysis, where internalized mutant-EGFR colocalized with pEGFR (Fig. 1A, bottom) whereas treatment with osimertinib blocked pEGFR staining (Supplementary Fig. S1F). These results suggest that mutant-EGFR forms are constitutively internalized and activated and suggest that mutant EGFR remains competent to signal from the endosomal compartment.

In order to investigate the impact of clathrin inhibition on mutant-EGFR localization and signaling, NSCLC cell lines were treated with the specific clathrin inhibitor pitstop (28) at a concentration that blocks totally the clathrin-dependent transferrin uptake (Supplementary Fig. S1G). Surprisingly, clathrin inhibition consistently leads to a significant decrease of the protein level of all mutant-EGFR (Fig. 1B) but not wild-type EGFR (Supplementary Fig. S1H and S1I) and transferrin receptor (TfnR; Supplementary Fig. S1J and S1K). In order to investigate the consequences of clathrin inhibition-induced mutant-EGFR degradation on receptor signaling, we first used the PC-9 cell line in which signaling is highly dependent on EGFR activation (Supplementary Fig. S1B). Results show that $EGFR^{ex19Del}$ degradation induced by clathrin inhibition is associated with a robust inhibition of EGFR phosphorylation tyrosine residues (Fig. 1C; Supplementary Fig. S1L) and an inhibition of EGFR-dependent signaling as shown with the significant decrease of pAKT or pERK (Fig. 1D). Similar results were observed for other mutants (Supplementary Fig. S1M–S1R). We then verified that the results obtained was not due to a nonspecific effect of pitstop2a using the two most-efficient siRNAs (based on the *P* value) to deplete clathrin heavy chain (CLTC; Supplementary Fig. S1S). CLTC siRNAs induced a significant decrease of EGFR protein level and phosphorylation, followed by a significant decrease of pAKT and pERK (Fig. 1E). These results support the importance of clathrin-mediated endocytosis (CME) for maintaining mutant-EGFR protein levels and signaling capability. In light of these unexpected findings, we postulated that clathrin inhibition resensitized mutant-EGFR degradation by redirecting the receptor toward a predominantly degradative pathway.

Clathrin inhibition induces mutant-EGFR degradation through lysosomal pathway

To test the hypothesis that clathrin inhibition diverts mutant-EGFR to the lysosomal pathway, we used chloroquine, a lysosome inhibitor that alkalinizes lysosomal pH, resulting in the upregulation of LC3a/b-II. Results show that in the presence of pitstop2, mutant-EGFR protein level is rescued in all cell lines tested when lysosomal function is disrupted with chloroquine (Fig. 2A–C; Supplementary Fig. S2A), thus suggesting that clathrin inhibition induces mutant-EGFR degradation through the lysosomal pathway. To further support this observation, we investigated mutant-EGFR localization by confocal microscopy in PC-9 cells. Following pitstop2 treatment alone, we observed a decrease of EGFR staining consistent with EGFR degradation under these conditions (Supplementary Fig. S2B). Furthermore, colocalization between EGFR and the lysosomal marker Lamp1 was barely observed, suggesting that $EGFR^{ex19Del}$ was already partly degraded. Instead, a pool of remaining $EGFR^{ex19Del}$ was colocalized with EEA1 (Supplementary Fig. S2B). By contrast, inhibition of CME with pitstop2, in the presence of chloroquine, induces an increased colocalization between EGFR and Lamp1 compared with chloroquine alone, supporting lysosomal degradation as the secondary pathway, and as such preventing endosomal signaling (Fig. 2D). Importantly, chloroquine-dependent mutant-EGFR protein level rescue was associated with recovery of receptor phosphorylation or mutant-EGFR–dependent signaling, as shown by the recovery of pERK and pAKT levels (Fig. 2E–G; Supplementary Fig. S2C–S2F). We verified that the signaling rescue was not due to a nonspecific effect of chloroquine by cotreating cells with osimertinib, and results showed that pAKT and pERK rescue were still dependent on mutant-EGFR activation (Supplementary Fig. S2G). These results indicate that following clathrin inhibition, mutant EGFR is diverted to the degradative lysosomal compartment via a clathrin-independent endocytosis (CIE) mechanism.

Mutant-EGFR lysosomal degradation induced by clathrin inhibition requires the macropinocytosis pathway

CIE has been associated with ligand-induced wild-type EGFR degradation, and proposed mechanisms of CIE include uptake via a cholesterol- and dynamin-dependent process (29, 30) or via a dynamin-independent process such as macropinocytosis (31). We, therefore, wished to determine which clathrin-independent endocytic pathway was primarily responsible for driving mutant-EGFR degradation following clathrin inhibition.

In order to discriminate those two different mechanisms, we first used dyngo4a to specifically inhibit dynamin (32) at a concentration that blocks totally the dynamin-dependent transferrin uptake (Supplementary Fig. S3A). Interestingly, the effect of dynamin inhibition on mutant-EGFR degradation was similar to that observed with clathrin inhibition (Supplementary Fig. S3B), suggesting the dynamin inhibition also redirects mutant-EGFR down a similar degradative process as clathrin inhibition, and thus this degradative pathway is also dynamin independent. Moreover, consistent with this premise, mutant-EGFR expression and signaling (pERK) was rescued with chloroquine treatment (Supplementary Fig. S3C and S3D) whereas no decrease was observed for wild-type EGFR (Supplementary Fig. S3E). Taken together, these observations by inference support the hypothesis that CIE mediating mutant-EGFR degradation is also a dynamin-independent process.

These observations lead to the hypothesis that macropinocytosis as being primarily responsible for mutant-EGFR degradative pathway. Macropinocytosis is a highly conserved endocytic actin-dependent process initiated from surface membrane ruffles that induces internalization of large endocytic vesicles called macropinosomes, which can also fuse with lysosomes (33). EIPA [5-(*N*-ethyl- *N*-isopropyl)-amiloride] is considered as the most specific macropinocytosis inhibitor (34) as it inhibits macropinocytosis without affecting other endocytic pathways (35).

In order to monitor mutant-EGFR internalization under clathrin and macropinocytosis inhibition, we took advantage of labeled EGF (EGF-Tritc) to stain the plasma membrane (PM) pool of the receptor. Briefly, after blocking the putative degradative pathways with pretreatment of chloroquine (to block

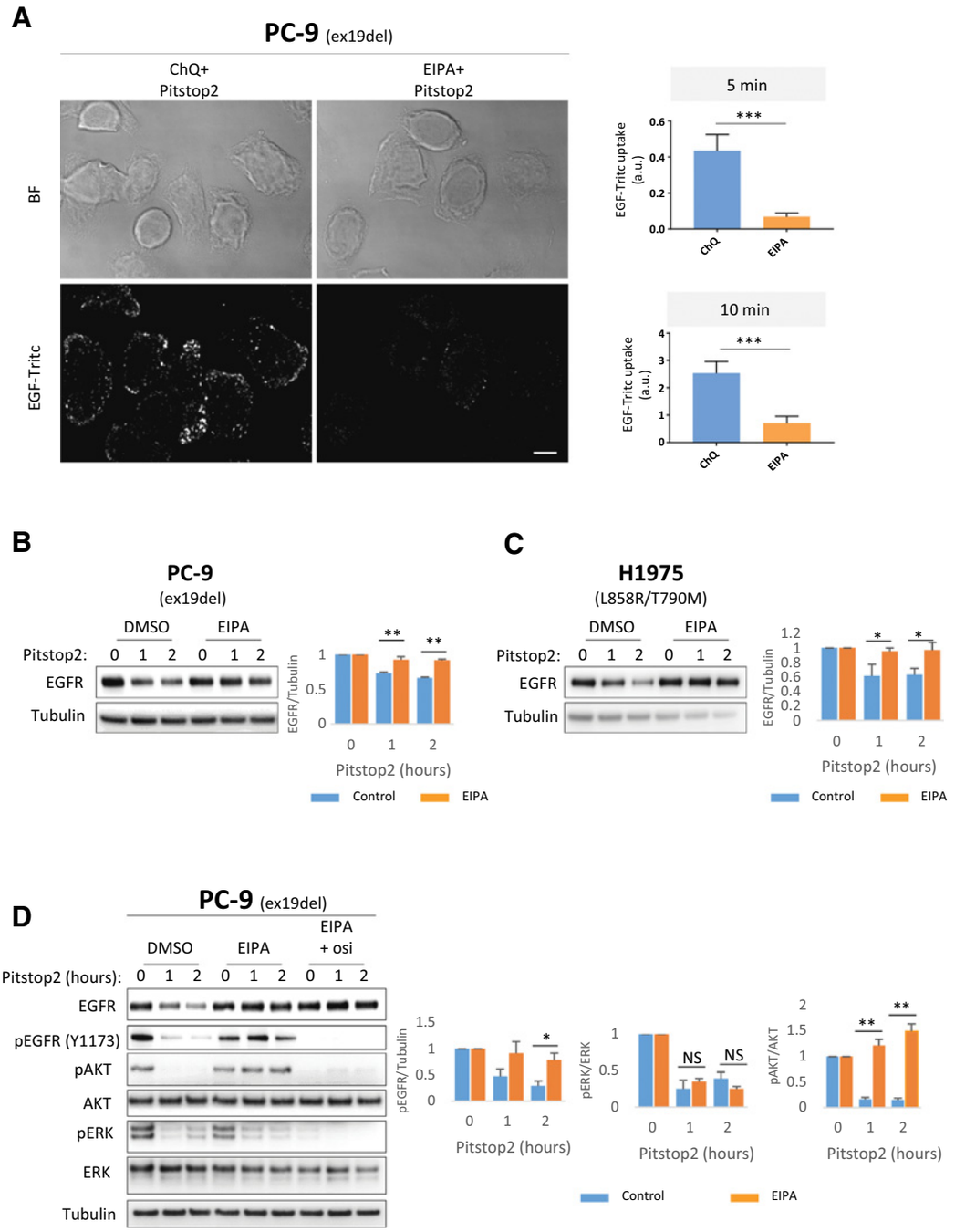

Figure 3.

Mutant-EGFR lysosomal degradation induced by clathrin inhibition requires the macropinocytosis pathway. **A,** Confocal sections and bright field of PC-9 cells treated with EGF-Tritc (white). Pictures are a magnification of the pictures shown in Supplementary Figure S3F. Cells were starved for 24 hours, pretreated with chloroquine (100 μmol/L) or EIPA (25 μmol/L) during 1 hour, followed by pitstop2 (30 μmol/L) treatment during 15 minutes at 37°C. Then, cells were incubated with EGF-Tritc (20 ng/mL) during 40 minutes at 4°C, washed and reincubated at 37°C during 5 or 10 minutes, and fixed. Pictures represent the 10-minute time point. Scale bar, 10 μm. Graphs represent the mean ± SEM of EGF-Tritc uptake ($n = 100$ cells; ***, $P < 0.001$, unpaired Student t test; a.u., arbitrary unit). **B,** PC-9 cells were starved during 24 hours and pretreated or not with EIPA (25 μmol/L) during 1 hour and treated with pitstop2 (30 μmol/L) for 1 and 2 hours. Western blots for EGFR and tubulin were performed. Fold decreases over pitstop2 untreated cells are shown. Data, means ± SEM ($n = 5$; *, $P < 0.05$; **, $P < 0.01$, Student t test). **C,** H1975 cells were starved during 24 hours and pretreated or not with EIPA (25 μmol/L) during 1 hour and treated with pitstop2 (30 μmol/L) for 1 and 2 hours. Western blots for EGFR and tubulin were performed. Fold decreases over pitstop2 untreated cells are shown. Data, means ± SEM ($n = 4$; *, $P < 0.05$, Student t test). **D,** PC-9 cells were starved during 24 hours, pretreated or not with osimertinib (160 nmol/L) during 15 minutes, followed by EIPA (25 μmol/L) treatment or not during 1 hour, followed with pitstop2 (30 μmol/L) treatment for 1 and 2 hours. Western blots for EGFR, pEGFR, pAKT (S473), AKT, pERK (T202/Y204), ERK, and tubulin were performed. Fold over untreated are shown. Data, means ± SEM ($n = 5$; *, $P < 0.05$; **, $P < 0.01$, NS, nonsignificant, Student t test).

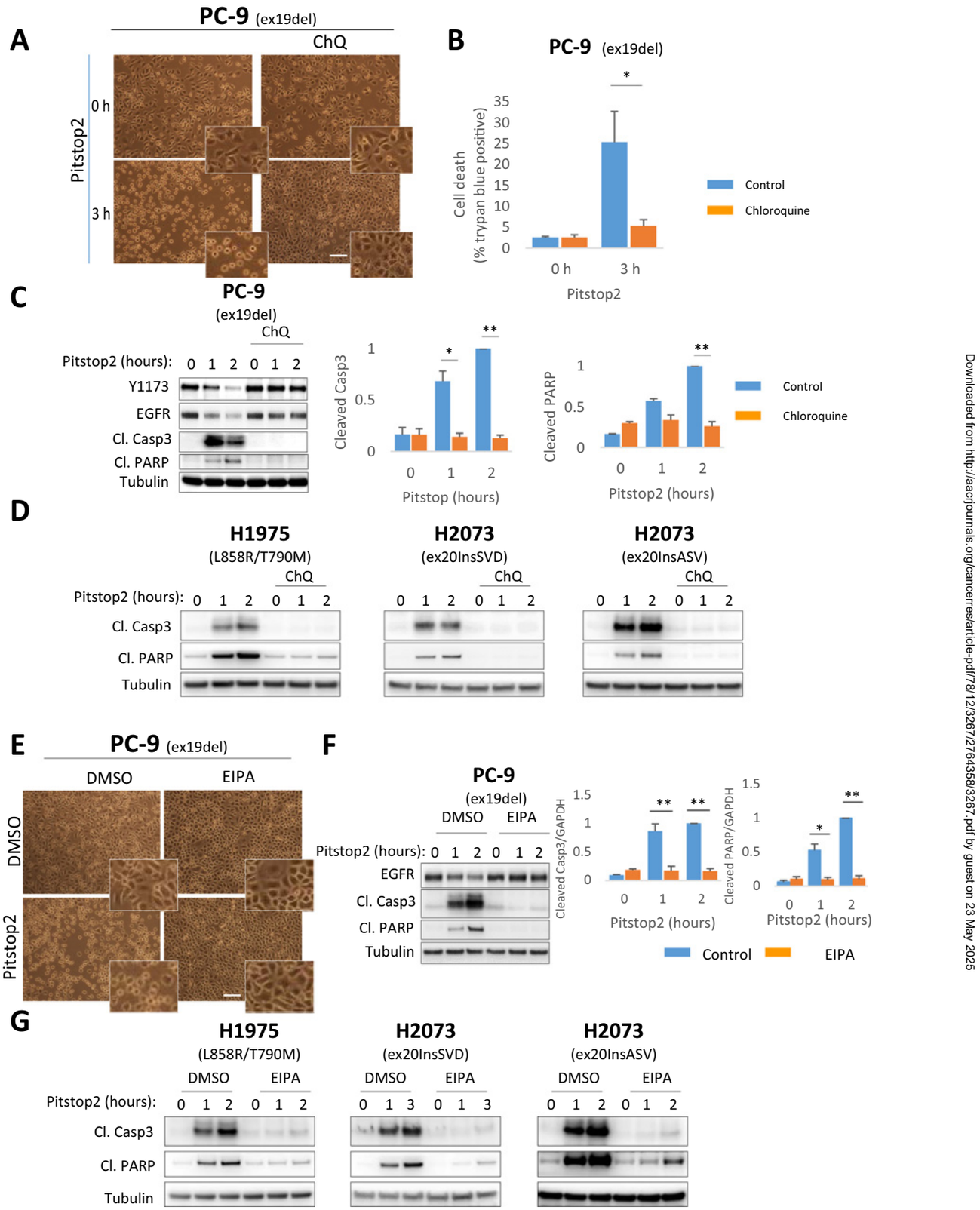

lysosomal degradation) or EIPA (to block macropinocytosis), followed by clathrin inhibition with pitstop2, cells were incubated at 4°C (to block internalization) with EGF-Tritc to stain the pool of mutant-EGFR trapped at the PM. Cells were then washed to remove the nonbound EGF-Tritc, and internalization of mutant-EGFR was transiently allowed by reincubating cells at 37°C during a short period (5 and 10 minutes; to diminish potential EGFR recycling to the PM). As shown on the confocal images and quantification, EGF-Tritc internalization was significantly inhibited in presence of EIPA versus chloroquine (5 and 10 minutes internalization; Fig. 3A; Supplementary Fig. S3F), indicating that clathrin-independent EGFR internalization occurs through macropinocytosis pathway. As a control, EGF-Tritc-labeled cells were fixed with paraformaldehyde directly after EGF-Tritc incubation at 4°C. Consistent with literature (36), results show that surface-bound EGF-Tritc was completely removed in this condition showing that detected EGF-Tritc correspond to the pool of mutant EGFR internalized from PM (Supplementary Fig. S3F, left). It, therefore, followed that blocking this macropinosome pathway after inhibition of CME should impair mutant-EGFR degradation. Indeed, results show that in presence of pitstop2, mutant-EGFR expression is rescued in NSCLC cell lines treated with the macropinocytosis inhibitor EIPA (Fig. 3B and C; Supplementary Fig. S3G). We then investigated the effect of EIPA on mutant-EGFR–dependent signaling in PC-9 cells, and importantly observed that EIPA treatment rescues pEGFR (Fig. 3D). Interestingly, whilst EIPA cotreatment also rescued pAKT signaling, pERK remained inhibited (Fig. 3D), suggesting that in PC-9 cells at least, mutant-EGFR localization influences downstream signaling, and PM localization is sufficient to activate more pAKT signaling than pERK. pAKT rescue was still dependent of mutant-EGFR activity as osimertinib blocked pAKT in presence of EIPA (Fig. 3D; Supplementary Fig. S3H). Taken together our results suggest that clathrin-independent mutant-EGFR degradation is associated with the macropinocytosis pathway.

CIE-induced mutant-EGFR degradation promotes apoptosis

As clathrin inhibition leads to degradation of mutant-EGFR and loss of signaling, we postulated whether this would in turn lead to loss of cell survival, and therefore provide a novel treatment approach across all forms of mutant-EGFR. As shown on bright field images (Fig. 4A), following pitstop2 treatment, PC-9 cells exhibited a rounding up and blebbing phenotype, indicative of cell death. This observation was supported by an increase of trypan blue uptake following pitstsop2 treatment, with 25% of positive cells compared with 2% for pitstop2 and control, respectively (Fig. 4B). Moreover, pitstop2 induced a robust induction of the apoptotic markers cleaved caspase-3 and cleaved PARP (Fig. 4C). As expected, the cell death observed following CME inhibition can be reverted by preventing EGFR degradation using chloroquine (Fig. 4A–C). Importantly, a similar phenotype was observed across the different mutant-EGFR–expressing NSCLC cell lines (Fig. 4D) whereas no effect was observed across cell lines expressing wild-type EGFR (Supplementary Fig. S4). Altogether, these results suggest that clathrin inhibition sensitizes mutant-EGFR cell lines to apoptosis, regardless of the EGFR mutation background.

Consistent with the proposed model of mutant-EGFR internalization via macropinocytosis being responsible for the cell death, EIPA treatment prevented the rounded phenotype of PC-9 cells induced by clathrin inhibition (Fig. 4E) and blocked completely the induction of cleaved caspase-3 and PARP (Fig. 4F). Similar results were obtained with cell lines expressing different mutant EGFR (Fig. 4G).

Clathrin inhibition induces degradation of mutant EGFR resistant to early and third-generation TKIs

In order to investigate whether our findings could be exploited to provide alternative treatment strategies to tackle EGFR-dependent resistance, we used a large panel of endogenous EGFR mutants including clinically relevant mutant EGFR resistant to osimertinib, still considered as an important clinical unmet need.

In order to demonstrate this proof of concept *in vitro*, we established isogenic PC-9 cell lines representing TKI-resistant mutations using CRISPR editing technology; $EGFR^{ex19del/T790M}$, $EGFR^{ex19del/C797S}$, and $EGFR^{ex19del/T790M/C797S}$ mutations. The isogenic cell lines showed the expected phenotypic and signaling sensitivity profiles to the different generation TKIs (Fig. 5A; Supplementary Fig. S5A and S5B). Consistent with earlier studies, all forms of mutant-EGFR across the isogenic lines were detected in intracellular vesicles, where a portion colocalized with the early endosomes marker EEA1 (Supplementary. Fig. S5C), suggesting that all TKI resistant mutants retain the ability to internalize in endosomal compartment. Importantly, pitstop2 inhibition of CME induced degradation across all the resistant mutant-EGFR variants, which was associated with loss of signaling and induction of cell death (Fig. 5b).

We then extended our findings to previously reported mutant-EGFR cell lines with acquired resistance to osimertinib independently of additional EGFR mutations such as C797S (26). Surprisingly, although short-term osimertinib treatment causes dephosphorylated mutant EGFR to relocate back to the plasma membrane in parental PC-9 and NCI-H1975 cell lines (Fig. 5C; Supplementary Fig. S5D and S5E), we observed that mutant EGFR within the osimertinib-resistant cell lines retained high levels of

Figure 4.

CIE-induced mutant-EGFR degradation promotes apoptosis. **A,** Bright field of PC-9 cells pretreated or not with chloroquine (100 μmol/L), followed by pitstop2 treatment (30 μmol/L) or not during 3 hours. Scale bar, 100 μm. **B,** Cell death of PC-9 cells after 3 hours of treatment with pitstop2 (30 μmol/L), pretreated or not with chloroquine (100 μmol/L). Cells were counted with automated cell counter Countess (Invitrogen) by Trypan blue exclusion. Data are means ± SEM, $n = 4$; *, $P < 0.05$. **C,** PC-9 cells were starved during 24 hours and pretreated or not with chloroquine (100 μmol/L) during 1 hour and treated with pitstop2 (30 μmol/L) for 1 and 2 hours. Western blots for EGFR, pEGFR, cleaved caspase-3 (Cl. Casp3), cleaved PARP, and tubulin were performed. Fold increases over untreated cells are shown. Data, means ± SEM ($n = 4$ for cleaved caspase-3; $n = 3$ for cleaved PARP; *, $P < 0.05$; **, $P < 0.01$, Student *t* test). **D,** Indicated cells were starved during 24 hours and pretreated or not with chloroquine (100 μmol/L) during 1 hour and treated with pitstop2 (30 μmol/L) for 1 and 2 hours. Western blots for cleaved caspase-3, cleaved PARP, and tubulin were performed. **E,** Bright field of PC-9 cells pretreated or not with EIPA (25 μmol/L) followed by pitstop2 treatment (30 μmol/L) or not during 2 hours. **F,** PC-9 cells were starved during 24 hours and pretreated or not with EIPA (25 μmol/L) during 1 hour and treated with pitstop2 (30 μmol/L) for 1 and 2 hours. Western blots for EGFR, cleaved caspase-3, cleaved PARP, and tubulin were performed. Fold increases over untreated cells are shown. Data, means ± SEM ($n = 5$ for cleaved caspase-3; $n = 4$ for cleaved PARP; *, $P < 0.05$; **, $P < 0.01$, Student *t* test). **G,** Indicated cells were starved during 24 hours and pretreated or not with EIPA (25 μmol/L) during 1 hour and treated with pitstop2 (30 μmol/L) for 1 and 2 hours. Western blots for cleaved caspase-3, cleaved PARP, and tubulin were performed.

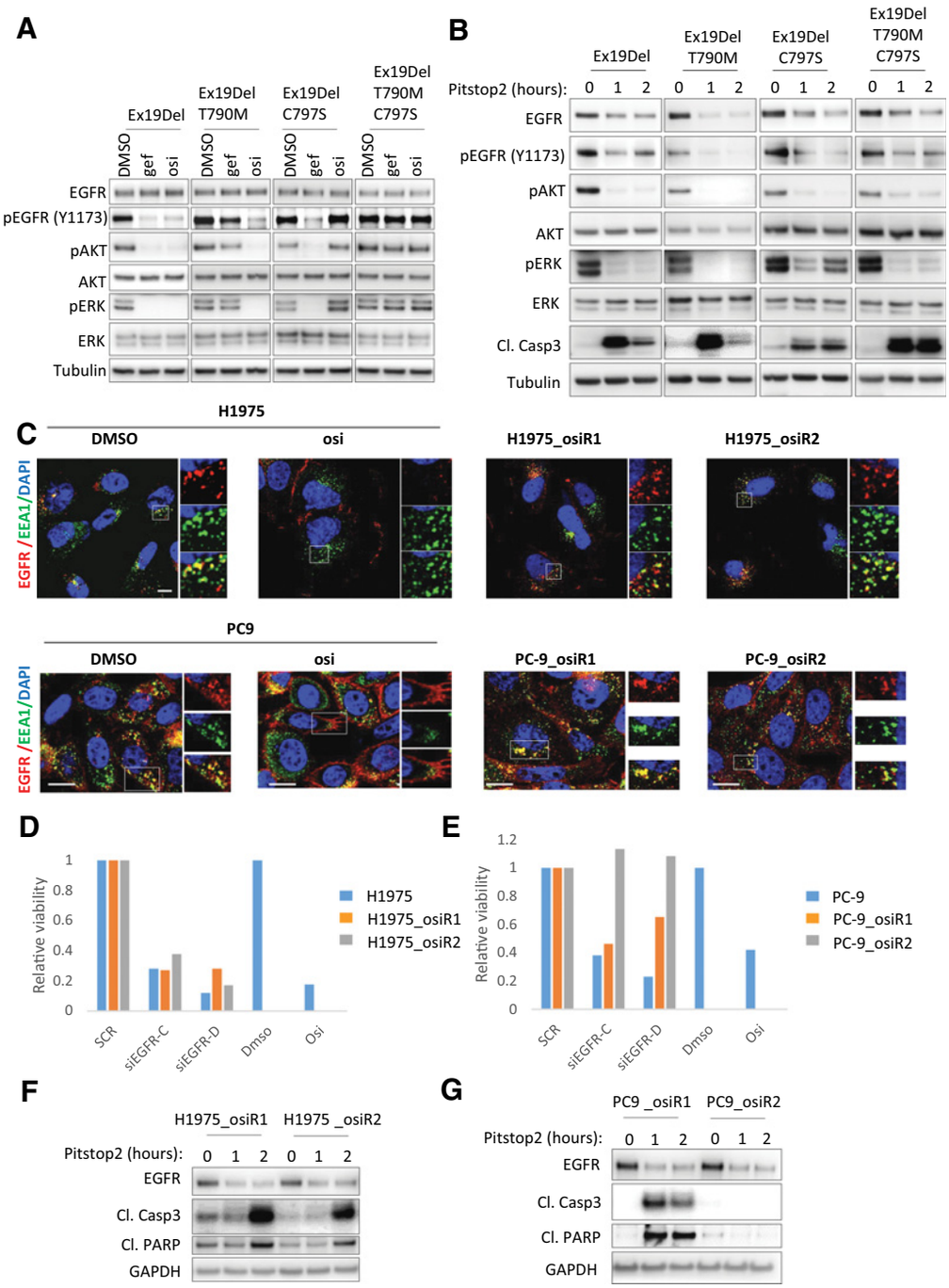

Figure 5.

Clathrin inhibition induces degradation of mutant-EGFR resistant to early and third-generation TKIs. **A,** Parental PC-9 and CRISPR-engineered EGFR mutant PC-9 cells were treated or not with gefitinib (160 nmol/L) or osimertinib (160 nmol/L) during 1 hour. Western blots for EGFR, pEGFR (Y1173), pAKT (S473), AKT, pERK (T202/Y204), ERK, and tubulin were performed. **B,** CRISPR-engineered EGFR mutant PC-9 cells were starved during 24 hours and pretreated or not with Pitstop2 (30 μmol/L) for 1 and 2 hours. Western blots for EGFR, pEGFR (Y1173), pAKT (S473), AKT, pERK (T202/Y204), ERK, cleaved caspase-3 (Cl. Casp3) and tubulin were performed. **C,** Confocal sections of parental and osimertinib-resistant cells stained for EGFR (red), EEA1 (green), and DAPI (blue). Parental cells were treated or not with 160 nmol/L of osimertinib during 2 hours 30 minutes and resistant cells were continuously maintained with 160 nmol/L of osimertinib. Scale bar, 10 μm. **D,** Relative viability of NCI-H1975 and osimertinib-resistant cells (NCI-H1975_osiR1 and NCI-H1975_osiR2) transfected with siEGFR, or siCt and treated or not with osimertinib (160 nmol/L). **E,** Relative viability of PC-9 and osimertinib-resistant cells (PC-9_osiR1 and PC-9_osiR2) transfected with siEGFR, or siCt and treated or not with osimertinib (160 nmol/L). **F,** Osimertinib-resistant NCI-H1975 cells were starved during 24 hours and treated or not with pitstop2 for 1 and 2 hours. Western blots for EGFR, cleaved PARP, cleaved caspase-3, and GAPDH were performed. **G,** Osimertinib-resistant PC-9 cells were starved during 24 hours and treated or not with pitstop2 for 1 and 2 hours. Western blots for EGFR, cleaved PARP, cleaved caspase-3, and GAPDH were performed.

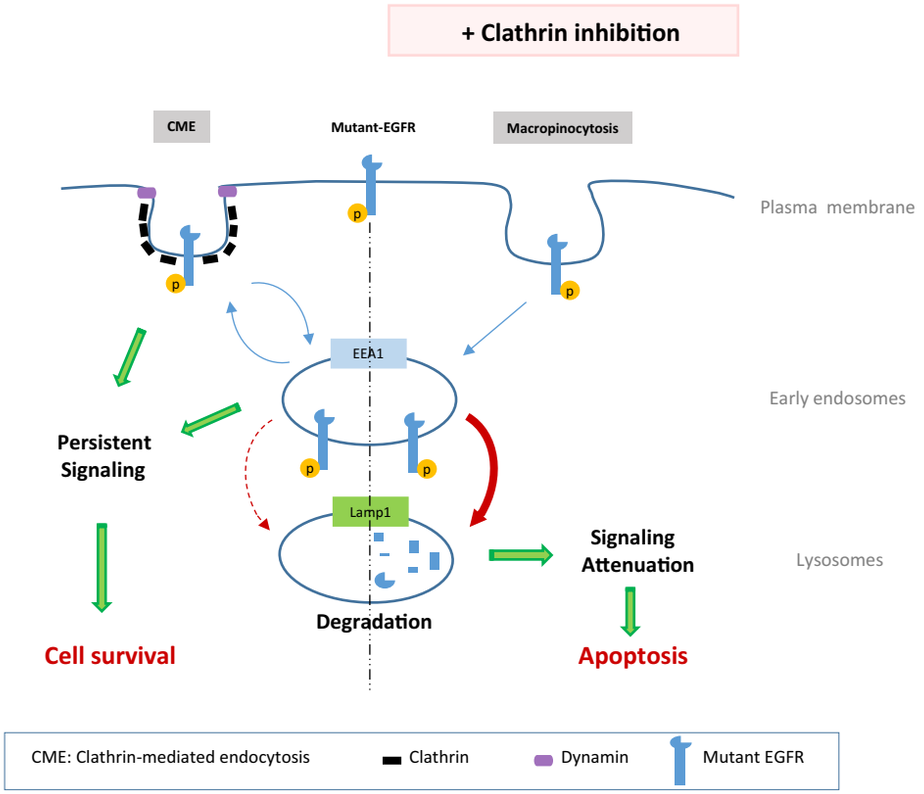

Figure 6.
Model. In cancer cells, internalized oncogenic mutant-EGFR forms via CME are not sorted to lysosomal degradation pathway, inducing a persistent signaling from PM and endosomal compartment, resulting in cell survival. Inhibition of CME induces a macropinocytosis-dependent mutant-EGFR internalization, followed by EGFR sorting to lysosomal compartment, where EGFR is degraded, resulting in signaling extinction and apoptosis.

basal endosomal internalization in presence of chronic osimertinib treatment, despite apparent lack of receptor phosphorylation (Fig. 5C; Supplementary Fig. S5D and S5E). This surprising observation indicated that mutant EGFR in osimertinib resistant cell context could reactivate its ability to traffic to subcellular compartments, and, we thus postulated that CME of EGFR could be contributing to osimertinib resistance. Indeed, knockdown of mutant EGFR with 2 different siRNAs inhibited cell viability of resistant cell lines to the same extent compared with parental cell lines, except for the PC-9_osiR2 cell line that showed an EGFR-independent resistance mechanism (Fig. 5D and E). Moreover, based on our model, we hypothesized that inhibition of clathrin would be sufficient to target-resistant EGFR for degradation. Crucially, pitstop2 treatment across all resistant cells induced mutant-EGFR degradation, which was associated with apoptosis induction of H1975_osiR1, H1975_osiR2, and PC-9_osiR1 cells, as shown by the cleavage of caspase-3 and PARP (Fig. 5F and G). Furthermore, consistent with its EGFR-independent resistance mechanism (Fig. 5E), pitstop2-induced mutant-EGFR degradation of PC-9_osiR2 was not sufficient to induce apoptosis (Fig. 5G).

Discussion

In normal cells, tight control of wild-type EGFR activation is thought to be the result of a balance between CME (associated to recycling and signaling sustainment) and CIE (associated to receptor degradation and signal extinction; ref. 37). In cancer cells, as mutant EGFR are constitutively internalized and are less sensitive to degradation (24, 25), we hypothesized that mutant-EGFR balance is deregulated and in favor of CME, and shifting that balance toward CIE trafficking through inhibition of CME, could provide a novel therapeutic approach to impair oncogenic functions of any mutant-EGFR variant. Moreover, this could provide a strategy to inhibit activating mutant EGFR that have become refractory to TKI inhibition, and pose a significant unmet medical need.

Our study showed for the first time that inhibition of CME using pitstop2 or clathrin siRNA redirects mutant EGFR to lysosomal degradation pathway, followed by rapid inhibition of signaling and induction of apoptosis (Fig. 6). Importantly, we have shown that mutant-EGFR degradation following inhibition of CME is a common mechanism across all the most clinically relevant TKI-sensitizing and resistance EGFR mutants that were tested; common activating mutations Ex19Del and L858R, uncommon Ex20Ins-activating mutants, EGFRm/T790M resistance mutation and osimertinib resistance C797S mutation (9). This suggests all constitutively active mutant-EGFR forms use the same trafficking mechanisms and is not specific to a particular EGFR mutation or cell background.

Our study is consistent with concept that mutant EGFR can be redirected to a CIE-degradative pathway also independent of dynamin, consistent with a previous study showing that CIE of activated wild-type EGFR is a dynamin-independent process (38). We have developed a model for mutant-EGFR trafficking, whereby under normal conditions, CME is the primary mechanism that supports signaling and survival functions of oncogenic EGFR. However, mutant-EGFR trafficking can be redirected toward a macropinocytosis-mediated degradative lysosomal CIE pathway if CME is blocked. Redirection of wild-type EGFR to CIE pathway also occurs after wild-type EGFR is stimulated with a high dose of EGF, resulting in the saturation of CME (37, 38). Recruitment into

CIE is tightly dependent on EGFR expression levels, as in cancer cells displaying high EGFR levels, phosphorylated wild-type EGFR is not coupled to ubiquitinylation, not targeted to CIE and thus not degraded (39). CIE regulation has also been associated with the type of EGFR ligand (40). It also remains unclear as to what mechanisms are responsible for CIE, and proposed mechanisms of CIE includes uptake via a cholesterol- and dynamin-dependent process (29, 30) or via macropinocytosis (31, 41). Discrepancies between dynamin-dependent and dynamin-independent CIE when comparing wild-type and mutant EGFR, respectively, are yet to be determined, but warrant further investigation. Moreover, future studies will be needed to further understand how the switch between CME and CIE is regulated depending on the context of EGFR.

As acquired resistance to EGFR-TKIs is inevitable, new strategies are needed to prolong benefit to patients and delay resistance. It is now clear that EGFR-dependent mechanisms account for a large proportion of TKI resistance, for example, T790M mutation following early generation TKIs (7, 42, 43) and C797S mutation following third-generation agents such as osimertinib (9). Other mechanisms of resistance, EGFR-dependent but without additional EGFR mutation, have been suggested and involve EGFR internalization and trafficking to specific subcellular localization in response to apoptotic inducers (44, 45). Interestingly, stress-induced EGFR internalization has often been shown to require CME and sometimes independently of its tyrosine kinase function (44, 45). Importantly, our results also show for the first time that a nonmutational EGFR osimertinib-resistance mechanism is possibly mediated through a reactivation of trafficking to subcellular compartments. To our knowledge, this is also the first evidence that resistance to a chronic treatment of osimertinib can still occur through unphosphorylated kinase domain of mutant EGFR suggesting a kinase-independent function of mutant EGFR in osimertinib resistance.

Consistent to this, other studies have reported kinase-independent functions of EGFR in cell survival (46) making it crucial to target both kinase-dependent and -independent functions. The data from this and previous studies indicates that mechanisms of resistance require EGFR internalization and trafficking, and functions seem associated with specific subcellular localizations, and thus we assessed the impact of mutant-EGFR degradation following clathrin inhibition in osimertinib resistant cell lines. As seen with EGFR containing resistance mutations, clathrin inhibition was sufficient to induce apoptosis in the osimertinib-resistant cell lines that had exhibited dependence on EGFR only.

Future studies will be needed to understand the noncatalytic and mutation-independent mechanisms by which EGFR can still contribute to osimertinib-acquired resistance.

Our findings have raised a number of novel and important insights. We have further developed our understanding of mutant-EGFR trafficking mechanisms. We propose the novel approach of exploiting these trafficking and degradation mechanisms of mutant EGFR to provide alternative treatment strategies to tackle EGFR-dependent resistance. And, we have identified that EGFR may be able to maintain a kinase-independent functional role for supporting acquired resistance to osimertinib, which may have dependency on endosomal trafficking.

As strategies focusing on reducing EGFR expression (siRNAs or proteolysis targeting chimeras) are so far unsuccessful, targeting clathrin-dependent endocytosis could be an interesting alternative therapeutic strategy for consideration. Interestingly, new inhibitor targeting the interaction between the clathrin adaptors, β2-arrestin, and AP2 (47), could offer new opportunity to target mutant EGFR to degradation in NSCLC, especially in the context of erlotinib resistance where members of AP2 family are overexpressed (23). Interestingly, as approved antipsychotic drugs such as chlorpromazine inhibit CME (48) and as cetuximab associated with anti-human IgG antibodies was shown to downregulate EGF-activated EGFR possibly through macropinocytosis (49), combination of these clinically available treatments, in the context of NSCLC expressing mutant EGFR, could potentially bring benefits to patients. As clathrin is important for endocytosis and signaling of many receptors (including other RTKs and GPCRs) generation of more specific inhibitors targeting specifically the EGFR region involved in CME may offer a new therapeutic avenue in cancer management.

Disclosure of Potential Conflicts of Interest

No potential conflicts of interest were disclosed.

Authors' Contributions

Conception and design: L. Ménard, N. Floc'h, D.A.E. Cross
Development of methodology: L. Ménard
Acquisition of data (provided animals, acquired and managed patients, provided facilities, etc.): L. Ménard, M.J. Martin
Analysis and interpretation of data (e.g., statistical analysis, biostatistics, computational analysis): L. Ménard, N. Floc'h, M.J. Martin, D.A.E. Cross
Writing, review, and/or revision of the manuscript: L. Ménard, N. Floc'h, M.J. Martin, D.A.E. Cross
Study supervision: D.A.E. Cross

Acknowledgments

The authors thank Daniel O'Neill and Emanuella Cuomo for the CRISPR cell line generation, other members of the Oncology Targets Biology group at AstraZeneca for technical assistance, and S. Kermorgant for critically reading the manuscript.

The costs of publication of this article were defrayed in part by the payment of page charges. This article must therefore be hereby marked *advertisement* in accordance with 18 U.S.C. Section 1734 solely to indicate this fact.

Received July 21, 2017; revised January 16, 2018; accepted March 14, 2018; published first March 19, 2018.

References

1. Pao W, Chmielecki J. Rational, biologically based treatment of EGFR-mutant non-small-cell lung cancer. Nat Rev Cancer 2010;10:760–74.
2. Sharma SV, Bell DW, Settleman J, Haber DA. Epidermal growth factor receptor mutations in lung cancer. Nat Rev Cancer 2007;7:169–81.
3. Arcila ME, Nafa K, Chaft JE, Rekhtman N, Lau C, Reva BA, et al. EGFR exon 20 insertion mutations in lung adenocarcinomas: prevalence, molecular heterogeneity, and clinicopathologic characteristics. Mol Cancer Ther 2013;12:220–9.
4. Mok TS, Wu YL, Thongprasert S, Yang CH, Chu DT, Saijo N, et al. Gefitinib or carboplatin-paclitaxel in pulmonary adenocarcinoma. N Engl J Med 2009;361:947–57.
5. Rosell R, Carcereny E, Gervais R, Vergnenegre A, Massuti B, Felip E, et al. Erlotinib versus standard chemotherapy as first-line treatment for European patients with advanced EGFR mutation-positive non-small-cell lung cancer (EURTAC): a multicentre, open-label, randomised phase 3 trial. Lancet Oncol 2012;13:239–46.

6. Chen D, Song Z, Cheng G. Clinical efficacy of first-generation EGFR-TKIs in patients with advanced non-small-cell lung cancer harboring EGFR exon 20 mutations. Onco Targets Ther 2016;9:4181–6.
7. Yu HA, Arcila ME, Rekhtman N, Sima CS, Zakowski MF, Pao W, et al. Analysis of tumor specimens at the time of acquired resistance to EGFR-TKI therapy in 155 patients with EGFR-mutant lung cancers. Clin Cancer Res 2013;19:2240–7.
8. Cross DA, Ashton SE, Ghiorghiu S, Eberlein C, Nebhan CA, Spitzler PJ, et al. AZD9291, an irreversible EGFR TKI, overcomes T790M-mediated resistance to EGFR inhibitors in lung cancer. Cancer Discov 2014; 4:1046–61.
9. Thress KS, Paweletz CP, Felip E, Cho BC, Stetson D, Dougherty B, et al. Acquired EGFR C797S mutation mediates resistance to AZD9291 in non-small cell lung cancer harboring EGFR T790M. Nat Med 2015;21:560–2.
10. Villasenor R, Kalaidzidis Y, Zerial M. Signal processing by the endosomal system. Curr Opin Cell Biol 2016;39:53–60.
11. Gould GW, Lippincott-Schwartz J. New roles for endosomes: from vesicular carriers to multi-purpose platforms. Nat Rev Mol Cell Biol 2009; 10:287–92.
12. Sorkin A, von Zastrow M. Endocytosis and signalling: intertwining molecular networks. Nat Rev Mol Cell Biol 2009;10:609–22.
13. Platta HW, Stenmark H. Endocytosis and signaling. Curr Opin Cell Biol 2011;23:393–403.
14. Sadowski L, Pilecka I, Miaczynska M. Signaling from endosomes: location makes a difference. Exp Cell Res 2009;315:1601–9.
15. Palamidessi A, Frittoli E, Garre M, Faretta M, Mione M, Testa I, et al. Endocytic trafficking of Rac is required for the spatial restriction of signaling in cell migration. Cell 2008;134:135–47.
16. Menard L, Parker PJ, Kermorgant S. Receptor tyrosine kinase c-Met controls the cytoskeleton from different endosomes via different pathways. Nat Commun 2014;5:3907.
17. Wang Y, Pennock S, Chen X, Wang Z. Endosomal signaling of epidermal growth factor receptor stimulates signal transduction pathways leading to cell survival. Mol Cell Biol 2002;22:7279–90.
18. Joffre C, Barrow R, Menard L, Calleja V, Hart IR, Kermorgant S. A direct role for Met endocytosis in tumorigenesis. Nat Cell Biol 2011;13:827–37.
19. Demory ML, Boerner JL, Davidson R, Faust W, Miyake T, Lee I, et al. Epidermal growth factor receptor translocation to the mitochondria: regulation and effect. J Biol Chem 2009;284:36592–604.
20. Cao X, Zhu H, Ali-Osman F, Lo HW. EGFR and EGFRvIII undergo stress- and EGFR kinase inhibitor-induced mitochondrial translocalization: a potential mechanism of EGFR-driven antagonism of apoptosis. Mol Cancer 2011;10:26.
21. Rao DS, Bradley SV, Kumar PD, Hyun TS, Saint-Dic D, Oravecz-Wilson K, et al. Altered receptor trafficking in Huntingtin Interacting Protein 1-transformed cells. Cancer Cell 2003;3:471–82.
22. Chen PH, Bendris N, Hsiao YJ, Reis CR, Mettlen M, Chen HY, et al. Crosstalk between CLCb/Dyn1-mediated adaptive clathrin-mediated endocytosis and epidermal growth factor receptor signaling increases metastasis. Dev Cell 2017;40:278–88 e275.
23. Saafan H, Foerster S, Parra-Guillen ZP, Hammer E, Michaelis M, Cinatl J Jr, et al. Utilising the EGFR interactome to identify mechanisms of drug resistance in non-small cell lung cancer - Proof of concept towards a systems pharmacology approach. Eur J Pharm Sci 2016;94:20–32.
24. Chung BM, Raja SM, Clubb RJ, Tu C, George M, Band V, et al. Aberrant trafficking of NSCLC-associated EGFR mutants through the endocytic recycling pathway promotes interaction with Src. BMC Cell Biol 2009; 10:84.
25. Shtiegman K, Kochupurakkal BS, Zwang Y, Pines G, Starr A, Vexler A, et al. Defective ubiquitinylation of EGFR mutants of lung cancer confers prolonged signaling. Oncogene 2007;26:6968–78.
26. Eberlein CA, Stetson D, Markovets AA, Al-Kadhimi KJ, Lai Z, Fisher PR, et al. Acquired resistance to the mutant-selective EGFR Inhibitor AZD9291 is associated with increased dependence on RAS signaling in preclinical models. Cancer Res 2015;75:2489–500.
27. Floc'h N, Martin MJ, Riess JW, Orme JP, Staniszewska AD, Menard L, et al. Anti-tumor activity of osimertinib, an irreversible mutant-selective EGFR tyrosine kinase inhibitor, in NSCLC harboring EGFR Exon 20 Insertions. Mol Cancer Thera 2018. pii: molcanther.0758.2017. doi: 10.1158/1535-7163.MCT-17-0758. [Epub ahead of print]
28. Robertson MJ, Deane FM, Stahlschmidt W, von Kleist L, Haucke V, Robinson PJ, et al. Synthesis of the Pitstop family of clathrin inhibitors. Nat Protoc 2014;9:1592–606.
29. Sigismund S, Woelk T, Puri C, Maspero E, Tacchetti C, Transidico P, et al. Clathrin-independent endocytosis of ubiquitinated cargos. Proc Natl Acad Sci U S A 2005;102:2760–5.
30. Caldieri G, Barbieri E, Nappo G, Raimondi A, Bonora M, Conte A, et al. Reticulon 3-dependent ER-PM contact sites control EGFR nonclathrin endocytosis. Science 2017;356:617–24.
31. Sorkin A, Goh LK. Endocytosis and intracellular trafficking of ErbBs. Exp Cell Res 2008;314:3093–106.
32. McCluskey A, Daniel JA, Hadzic G, Chau N, Clayton EL, Mariana A, et al. Building a better dynasore: the dyngo compounds potently inhibit dynamin and endocytosis. Traffic 2013;14:1272–89.
33. Racoosin EL, Swanson JA. Macropinosome maturation and fusion with tubular lysosomes in macrophages. J Cell Biol 1993;121:1011–20.
34. Commisso C, Davidson SM, Soydaner-Azeloglu RG, Parker SJ, Kamphorst JJ, Hackett S, et al. Macropinocytosis of protein is an amino acid supply route in Ras-transformed cells. Nature 2013;497:633–7.
35. West MA, Bretscher MS, Watts C. Distinct endocytotic pathways in epidermal growth factor-stimulated human carcinoma A431 cells. J Cell Biol 1989;109:2731–9.
36. Pinilla-Macua I, Sorkin A. Methods to study endocytic trafficking of the EGF receptor. Methods Cell Biol 2015;130:347–67.
37. Sigismund S, Argenzio E, Tosoni D, Cavallaro E, Polo S, Di Fiore PP. Clathrin-mediated internalization is essential for sustained EGFR signaling but dispensable for degradation. Dev Cell 2008;15:209–19.
38. Jiang X, Sorkin A. Epidermal growth factor receptor internalization through clathrin-coated pits requires Cbl RING finger and proline-rich domains but not receptor polyubiquitylation. Traffic 2003;4:529–43.
39. Capuani F, Conte A, Argenzio E, Marchetti L, Priami C, Polo S, et al. Quantitative analysis reveals how EGFR activation and downregulation are coupled in normal but not in cancer cells. Nat Commun 2015;6:7999.
40. Henriksen L, Grandal MV, Knudsen SL, van Deurs B, Grovdal LM. Internalization mechanisms of the epidermal growth factor receptor after activation with different ligands. PLoS One 2013;8:e58148.
41. Barbieri E, Di Fiore PP, Sigismund S. Endocytic control of signaling at the plasma membrane. Curr Opin Cell Biol 2016;39:21–7.
42. Pao W, Miller VA, Politi KA, Riely GJ, Somwar R, Zakowski MF, et al. Acquired resistance of lung adenocarcinomas to gefitinib or erlotinib is associated with a second mutation in the EGFR kinase domain. PLoS Med 2005;2:e73.
43. Sequist LV, Waltman BA, Dias-Santagata D, Digumarthy S, Turke AB, Fidias P, et al. Genotypic and histological evolution of lung cancers acquiring resistance to EGFR inhibitors. Sci Transl Med 2011;3:75ra26.
44. Tomas A, Vaughan SO, Burgoyne T, Sorkin A, Hartley JA, Hochhauser D, et al. WASH and Tsg101/ALIX-dependent diversion of stress-internalized EGFR from the canonical endocytic pathway. Nat Commun 2015;6:7324.
45. Zwang Y, Yarden Y. p38 MAP kinase mediates stress-induced internalization of EGFR: implications for cancer chemotherapy. EMBO J 2006; 25:4195–206.
46. Tan X, Lambert PF, Rapraeger AC, Anderson RA. Stress-Induced EGFR trafficking: mechanisms, functions, and therapeutic implications. Trends Cell Biol 2016;26:352–66.
47. Beautrait A, Paradis JS, Zimmerman B, Giubilaro J, Nikolajev L, Armando S, et al. A new inhibitor of the beta-arrestin/AP2 endocytic complex reveals interplay between GPCR internalization and signalling. Nat Commun 2017;8:15054.
48. Daniel JA, Chau N, Abdel-Hamid MK, Hu L, von Kleist L, Whiting A, et al. Phenothiazine-derived antipsychotic drugs inhibit dynamin and clathrin-mediated endocytosis. Traffic 2015;16:635–54.
49. Berger C, Madshus IH, Stang E. Cetuximab in combination with anti-human IgG antibodies efficiently down-regulates the EGF receptor by macropinocytosis. Exp Cell Res 2012;318:2578–91.